Lead adsorption on the Al13Co4(100) surface: heterogeneous nucleation and pseudomorphic growth

Rafik Addou, Ankit Shukla, Sebastian Alarcon Villaseca, Emilie Gaudry,
Thomas Deniozou, Marc Heggen, Michael Feuerbacher, Remo N Widmer,
Oliver Gröning, Vincent Fournée, et al.

New Journal of Physics

Lead adsorption on the $Al_{13}Co_4$(100) surface: heterogeneous nucleation and pseudomorphic growth

R Addou[1], **A K Shukla**[1], **S Alarcón Villaseca**[1], **É Gaudry**[1], **Th Deniozou**[1], **M Heggen**[2], **M Feuerbacher**[2], **R Widmer**[3], **O Gröning**[3], **V Fournée**[1], **J-M Dubois**[1] and **J Ledieu**[1,4]

[1] Institut Jean Lamour (UMR 7198 CNRS-Nancy-Université-UPV-Metz), Ecole des Mines, Parc de Saurupt, 54042 Nancy Cedex, France
[2] Institut für Festkörperforschung, Forschungszentrum Jülich, 52425 Jülich, Germany
[3] Empa, Swiss Federal Laboratories for Materials Testing and Research, nanotech@surfaces Laboratory, Feuerwerkerstrasse 39, CH-3602 Thun, Switzerland
E-mail: Julian.ledieu@ijl.nancy-universite.fr

Abstract. We have investigated the adsorption of Pb atoms on the (100) surface of an orthorhombic $Al_{13}Co_4$ crystal at 300 and 573 K substrate temperatures. This complex metallic alloy is an approximant to the decagonal Al–Ni–Co quasicrystal. At submonolayer coverage and at 300 K, Pb adatoms remain highly mobile and adsorb preferentially within the hollow site situated in between adjacent Al pentagonal clusters present at the surface. These experimental findings are supported by *ab initio* calculations based on density functional theory (DFT). For both temperature regimes, Pb adsorption leads to the formation of pseudomorphic monolayers above which the high adsorbate mobility prohibits the growth of additional layers. For the high-temperature deposition, we propose a structural model for the Pb film and discuss its relationship with the underneath substrate.

[4] Author to whom any correspondence should be addressed.

IOP Institute of Physics Φ DEUTSCHE PHYSIKALISCHE GESELLSCHAFT

Contents

1. Introduction

When dealing with complex metallic alloy (CMA) systems such as aperiodic phases, a complete understanding is still lacking on how the chemical and/or structural complexities influence the alloy physical properties. There exist different approaches to partially disentangle one contribution from the other, hence facilitating the study of their individual role. In recent years, considerable attention has been focused for instance on finding quasicrystals with a less complex chemical composition. A major step towards that direction was made with the recent discovery of a stable icosahedral binary quasicrystal [1, 2]. Another alternative relies on the use of quasicrystal surfaces as templates for the growth of single-element pseudomorphic thin films [3–12]. Such films are of particular interest as they provide an opportunity to study the aperiodic order without the associated chemical complexity. Recently, Pb adsorption on various Al-rich quasicrystalline surfaces resulted in the formation of a quasiperiodic Pb monolayer (ML) [10, 13–15]. The initial choice of Pb as adsorbate was driven by its low elemental surface energy compared to Al(111) crystal [16] and its immiscibility with Al, hence reducing the possibility of intermixing phenomena and surface alloy formation.

The first study of Pb deposition on a quasicrystalline surface (icosahedral $Al_{70}Pd_{21}Mn_9$) was conducted by Ledieu *et al* [10] using scanning tunnelling microscopy (STM) and scanning tunnelling spectroscopy (STS), low-energy electron diffraction (LEED), x-ray photoelectron spectroscopy (XPS) and ultraviolet photoelectron spectroscopy (UPS). It was shown that the quasiperiodic Pb ML can be formed within a broad range of temperatures from 57 to 653 K. Its structural quality is improved upon subsequent annealing below 653 K. The density of the Pb ML (0.09 atom $Å^{-2}$) has been found to be very similar to the density of 1 ML Pb adsorbed on an Al(111) surface. This quasiperiodic Pb ML exhibits properties that are fundamentally different from those of bulk Pb. The most striking evidence is the presence of a wide *pseudo*-gap in the electronic density of states (DOS) at E_F observed by STS and UPS. The structure of the ML is τ-inflated compared to the surface structure of the substrate.

Similarly, the growth of Pb on the 10-f surface of the d-$Al_{72}Ni_{11}Co_{17}$ quasicrystal at room temperature has been studied using STM and LEED [13]. The adsorption leads also to the formation of a well-ordered quasiperiodic overlayer of Pb on this quasicrystal surface. As in the

Pb/i-Al–Pd–Mn study, pentagonal features of dimensions 4.9 Å are discernible within the first ML. However, the growth mechanism of the first ML in the Pb/d-Al–Ni–Co system is different from that of the Pb/i-Al–Pd–Mn case. The first ML of Pb on the i-Al–Pd–Mn self-assembles via a network of pentagonal islands. These fivefold clusters are a consequence of a heterogeneous nucleation of Pb adatoms at sub-ML coverage [14]. On the d-Al–Ni–Co surface, the growth proceeds with the lateral expansion of Pb islands instead of the formation of a dispersed network of pentagonal clusters as seen on the i-Al–Pd–Mn substrate. Therefore, the STM data suggest a higher diffusion length for adsorbing Pb atoms on the 10-f compared to the 5-f quasicrystalline surface.

In addition, the growth of Pb thin films has been carried out on the 5-f surface of the i-Al$_{63}$Cu$_{24}$Fe$_{13}$ quasicrystal [15]. Here again, the ML exhibits a quasiperiodic ordering and the nucleation is characterized as heterogeneous, i.e. Pb atoms nucleate at a specific adsorption site. XPS measurements show consistently throughout these studies that there is hardly any shift in the Al and Pb core levels with increasing deposition of Pb, indicative of a weak Pb and Al atom interaction [10, 13, 15]. For these three quasicrystalline substrates, the growth of additional layers is precluded upon completion of the τ inflated pseudomorphic ML. Interestingly, the scenario is different for the growth of Pb on ordinary metals. For example, the growth mode of Pb on Al(111) is of Frank–Van der Merwe type (layer-by-layer) [15]. The relatively weak interaction between Pb adatoms and the Al(111) substrate generates a moiré structure. Moreover, the growth of Pb on Cu(111) develops into three-dimensional (3D) islands due to quantum size effects [17]. Differences in the behaviour of Pb on quasicrystalline and metallic substrates may be correlated to the quasicrystal structural complexity compared to 'ordinary' periodic crystals. An alternative explanation for the apparent 'non-stick' behaviour of Pb adatoms would be fast diffusion of the adsorbate on the wetting layer, leading to the formation of Pb mounds separated by large distances and hardly detectable by STM or XPS measurements.

Although chemically and structurally closely related, approximant systems are less complex than quasicrystals as they possess a finite-size unit cell. On the other hand, approximants remain much more complex than usual elemental metals due to their giant unit cell, whose basis structure is best characterized using highly symmetric clusters. In this paper, Pb deposition on the Al$_{13}$Co$_4$(100) approximant surface provides an opportunity to study the adsorption on a surface that is structurally intermediate to elemental metals and quasicrystals. This work will also be important for assessing the influence of clusters present within the topmost surface layers on the adsorbate growth mode. The experimental details will be presented in section 2.1. Then, the adsorption of Pb adatoms on the pseudo-tenfold (*p*-10f) surface of the Al$_{13}$Co$_4$ crystal at room temperature and at 573 K will be described in section 3. Finally, the main results will be discussed in section 4.

2. Experimental and computational details

2.1. Experimental details

The *p*-10f surface of the Al$_{13}$Co$_4$, approximant to the decagonal quasicrystal, has been used as a substrate for Pb deposition. The Al$_{13}$Co$_4$ single crystal was grown by means of the Bridgman technique. The quality of the material was characterized by phase-contrast optical microscopy, scanning electron microscopy and transmission electron microscopy. The preparation procedure

IOP Institute of Physics Φ DEUTSCHE PHYSIKALISCHE GESELLSCHAFT

applied to the surface includes cycles of Ar$^+$ ion sputtering followed by annealing cycles [18]. The cleanliness, topography and the overall structure of the surface were checked using XPS, STM and LEED. The surface structural quality was systematically verified prior to depositions. Lead adsorption was carried out at room temperature using an Omicron electron beam cell that is flux monitored. The deposition rate was calibrated using STM by measuring the fractional area covered with successive Pb depositions. The flux was set to 4.2×10^{-3} ML s^{-1} throughout this study. The pressure during depositions was kept in the low 10^{-10} mbar range. The STM studies were performed at room temperature in constant current mode using an Omicron variable-temperature STM. XPS experiments were carried out using a non-monochromatized MgK$_\alpha$ source (1253.6 eV).

2.2. Computational details

The present *ab initio* calculations, based on the density functional theory (DFT) framework, have been performed with the Vienna *ab initio* simulation package (VASP) [19, 20] using the projector-augmented wave (PAW) method [21, 22] to describe the interaction between the valence electrons and the ionic core. Electronic exchange and correlation are described by the generalized gradient approximation PBE proposed in [23, 24]. The optimization of the atomic coordinates (and unit cell dimensions for bulk material) is performed via the calculation of the Hellmann–Feynman forces acting on atoms and their minimization via a conjugate gradient algorithm. Simulations are achieved by building non-symmetric six-layer thick slabs separated by a 15 Å-thick vacuum region. The two atomic layers at the bottom are kept fixed while the other four layers are allowed to relax. Such a small slab thickness is not satisfactory to get well-converged adsorption energies. Nevertheless, tests performed with six-layer and eight-layer thick slabs (corresponding to a total thickness of 11.5 and 16.0 Å, respectively) indicate that despite differences in the absolute values of the calculated adsorption energies ($\simeq 50$ meV), the adsorption energy differences between two distinct adsorption sites are small ($\leqslant 100$ meV within the tested sites), the adsorption geometry being almost identical.

Adsorption studies are conducted on the surface structure models that were determined in a previous work combining experimental (dynamical LEED and STM) and computational results [25]. More precisely, the surface structural model is built from a bulk truncation. The topmost atomic layer consists of an incomplete puckered layer where Co atoms have been removed from the surface. The resulting surface termination is schematically represented in the figure inserted in table 1. Two types of bipentagonal patterns, each composed of ten Al atoms, can be identified on the model, along with the two Al atoms referred to as 'glue' atoms. The bipentagonal pattern which is above the mean position of the topmost surface layer will be referred to as the 'protruding' one.

3. Results

3.1. The Al$_{13}$Co$_4$(100) clean surface

The investigation of the (100) surface of the Al$_{13}$Co$_4$ has been reported recently by Addou *et al* [18]. The LEED pattern and the XPD measurements recorded from the clean surface along with the single scattering cluster (SSC) calculations confirm the *p*-10f symmetry of the Al$_{13}$Co$_4$(100) surface. The STM image (figure 1(a)) reveals a step-terrace like morphology with terraces of lateral dimensions of the order of 100 nm. The step height measured between

Table 1. Relative adsorption energies of different sites selected on the S_2 structural model of the (100) surface of o-$Al_{13}Co_4$ ($\Delta E = E^i - E^4$, where E^i (resp. E^4) is the adsorption energy of site i (resp. 4)). Al atoms belonging to the bipentagonal pattern slightly above the mean position of the topmost atomic layer ('protruding') are shown in dark blue (black), while the Al atoms belonging to the bipentagonal pattern slightly below the mean position of the topmost atomic layer are shown in green (grey). The two Al glue atoms are represented by circles.

| Site	ΔE (eV)
1	0.39
2	0.01
3	0.69
4	0.00
5	−0.10
6	0.05
7	0.02
8	0.05
9	0.66
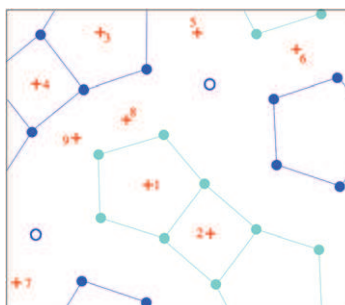
successive terraces is equal to 4.20 ± 0.20 Å. It was found that two types of surface terminations, referred as T1 and T2, could coexist on terraces. However, the surface preparation leads to an incomplete or patches of T2 at the surface (see figures 1(a) and (b)). The bulk model can be described as a sequence of two types of planes along the [100] direction: a flat (F) and a puckered (P) layer[5]. It has been demonstrated that T2 corresponds to an incomplete F plane, while T1 is associated with an incomplete P plane. For illustration purposes, a complete puckered plane is presented in figure 1(c). Depending on the position of the Co atoms (above or below the Al pentagons), two types of bipentagonal motifs can be distinguished and have been outlined in figure 1(c). The Al pentagons sitting above (below) the Co atom are located above (below) the mean position of the P plane. Using higher-resolution STM images, Addou *et al* [18] have shown that the brightest features observed on T1 are related to the 'protruding' bipentagonal motifs, leading indeed to a higher STM signal. Complementarily to this STM work, a recent dynamical LEED analysis carried out on this surface has led to the structural model presented in figure 9(b) [25]. The latter consists of a puckered layer where all Co atoms have been removed, hence leaving a T1 termination as consisting of 22 Al atoms per surface unit cell. As mentioned in section 2.2, this is the model used for the *ab initio* calculations (see figure 9(b) and the model in table 1).

3.2. Pb deposition at 300 K

3.2.1. Low-energy electron diffraction analysis. Figure 2 shows the LEED patterns recorded for the clean surface of the $Al_{13}Co_4$ sample and after successive (1–12 ML equivalent (MLE))

---

[5] T1 and T2 terminations correspond to incomplete puckered (P) and flat (F) layers, respectively. The orthorhombic $Al_{13}Co_4$ structure can be described by a stacking of P and F layers ($F_{0.0}P_{0.25}F_{0.5}P_{0.75}$ sequence) along the [100] direction.
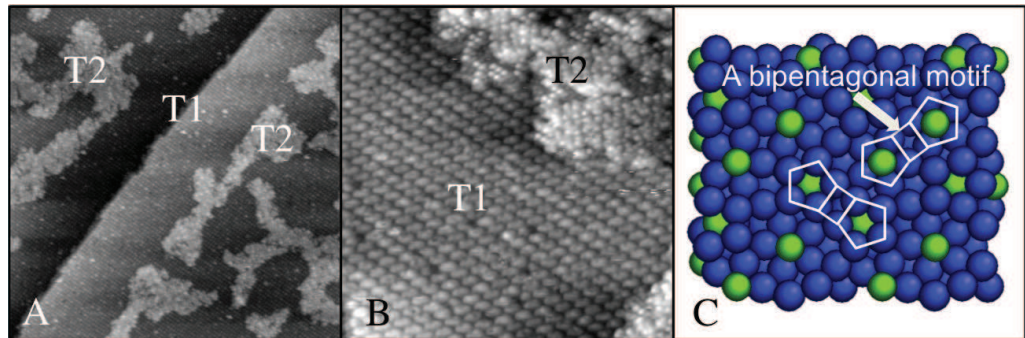
Figure 1. (a) 70 nm × 70 nm STM image showing the coexistence of T1 (large terraces) and T2 (resembling islands) layers. (b) This (35 nm × 35 nm) STM image allows us to appreciate the different atomic arrangements between T1 and T2 terminations. (c) The atomic model corresponding to a complete puckered layer present in the bulk model. The blue (dark) and green (light) spheres correspond to Al and Co atoms, respectively.
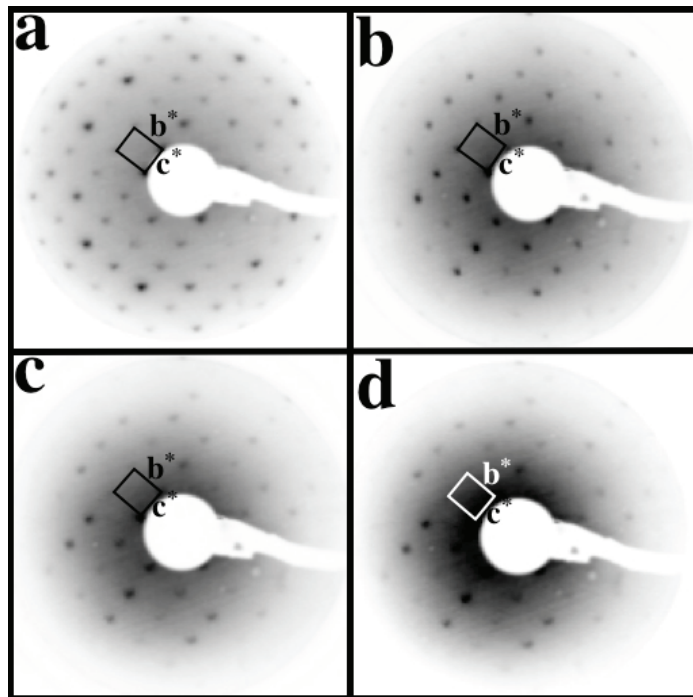
Figure 2. LEED patterns (inverted for clarity) recorded at 40 eV as a function of Pb exposure on the $Al_{13}Co_4(100)$ surface: (a) clean, (b) 2 MLE, (c) 7 MLE and (d) 12 MLE.

Pb exposures. The term MLE refers here to a coverage of one ML determined using STM by measuring the fractional area covered with successive Pb depositions and by considering a linear increase of Pb in the sub-ML regime as measured using XPS (see figure 7(a)). The orthorhombic structure of the clean $Al_{13}Co_4$ surface is evident from the diffraction pattern shown in figure 2(a). Within the accuracy of our measurements, the measured lattice parameter
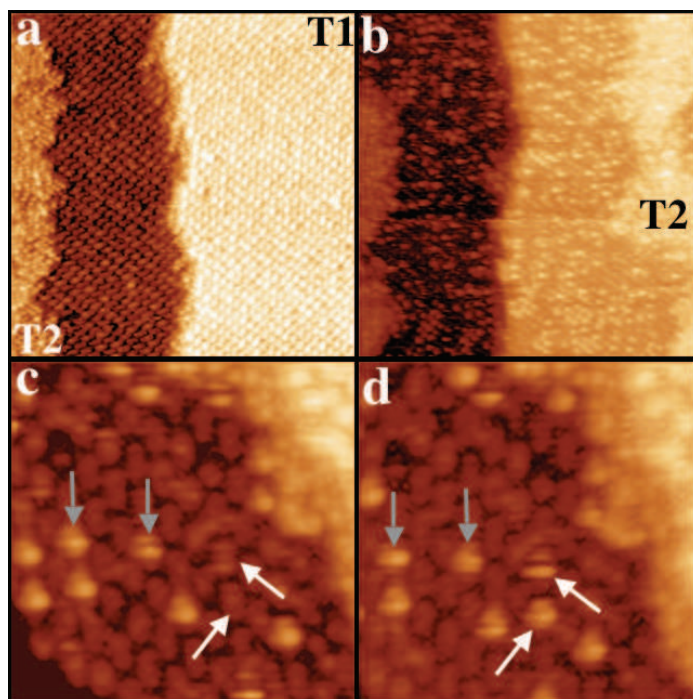
Figure 3. (a) STM image of the clean $Al_{13}Co_4$ substrate $(50 \times 50 \, nm^2)$. (b) STM image recorded after deposition of 0.13 MLE of Pb at room temperature $(100 \times 100 \, nm^2)$; (c, d) comparison of two STM images $(15 \times 15 \, nm^2)$ recorded successively on the same region and for the same coverage. The white (grey) arrows point to Pb atoms which have moved (not moved) during the scan.

dimensions are consistent with those reported by Grin *et al* [26] for the bulk model. As shown in figure 2(b), the diffraction pattern stays reasonably sharp up to 2 MLE dosage with a low to medium background. Upon additional Pb exposure, the patterns start to degrade with a clear background increase. However, the overall orthorhombic structure is still preserved even for the highest exposure (see figure 2(d)). At each stage of the deposition, the mesh of the reciprocal lattice vectors remains unchanged. As explained in the following section, the LEED measurements are consistent with the STM observations which indicate the growth of a pseudomorphic ML followed by the formation of large Pb clusters at step bunches, hence leading to a reduced quality of the LEED pattern for the highest exposures used in this study.

3.2.2. Scanning tunnelling microscopy measurements. After annealing the sample to 1120 K for 1 h, a majority of the clean $Al_{13}Co_4$ surface consists of relatively narrow terraces with T1 termination as the dominant topmost surface layer [18]. Figure 3(a) presents an STM image of the clean $Al_{13}Co_4$ surface prior to Pb dosing. While a majority of the terraces are indeed composed of T1 termination, a small fraction of the image is covered by T2 termination. Annealing to higher temperatures (1173 K) leads to a surface exclusively terminated by T1 layers. Figure 3(b) shows an STM image recorded after the deposition of 0.13 MLE of Pb at 300 K. Within this sub-ML regime, the adsorbates remain highly mobile (see figures 3(c)
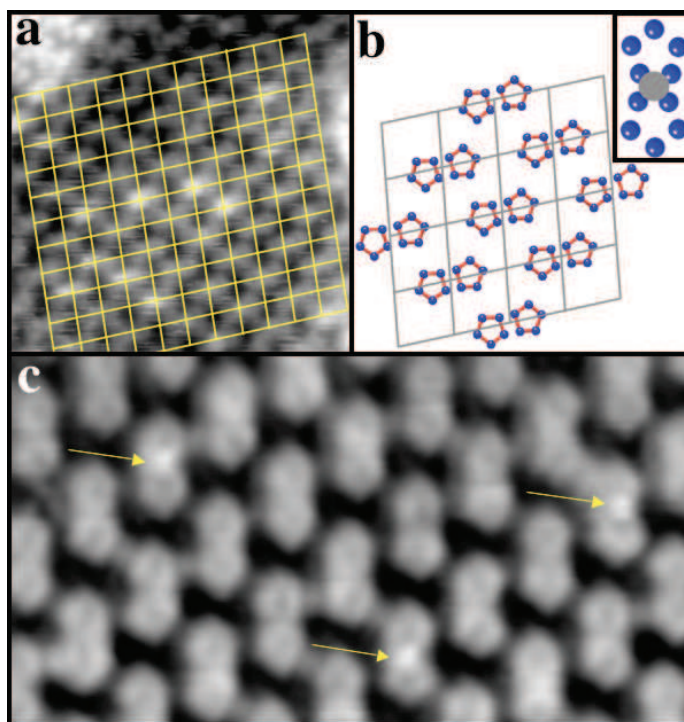
Figure 4. (a) STM image $(15 \times 15\,\text{nm}^2)$ recorded after dosing $0.38\,\text{MLE}$ of Pb at $300\,\text{K}$ on the $\text{Al}_{13}\text{Co}_4$ substrate. A grid representing the diagonals of the orthorhombic unit cell has been superimposed on this STM image. (b) Schematic representation of the superposition of the grid above the incomplete P layer (T1 termination) [26]. Only the 'protruding' bipentagonal motifs are shown. Inset: the large grey circle indicates the preferential adsorption site of Pb atoms as deduced from (a). (c) STM image $(11 \times 6\,\text{nm}^2)$ of the clean $\text{Al}_{13}\text{Co}_4$ surface. The arrows indicate that extra atoms (intrinsic or impurities) remaining after the standard surface preparation nucleate preferentially in the middle of the bipentagonal motifs, i.e. as for Pb adatoms.

and (d)) but there is no sign of cluster or island formation. While the adsorbates are easily distinguishable on T1, it is rather difficult to estimate the number of Pb atoms located on the T2 region. Because of the low density of this region, Pb adatoms decorating the edges and/or filling several interstices of the T2 layer remain strong possibilities. However, the adsorbates do not nucleate on top of T2 termination (no height difference measured).

We now focus on Pb adsorption on the T1 region and compare STM images recorded successively on the same region (figures 3(c) and (d)). From the two possible sets of bipentagonal motifs present within the puckered layer [25], the 'protruding' ones characteristic of the incomplete puckered plane (see [18]) are still well resolved in both STM images. Individual Pb adatoms that appear as bright protrusions in the images are located on top of the bipentagonal motifs. This is also supported by the distances measured between individual atoms, which correspond to multiples of the lattice parameters along the b- and the c-axis. Hence, Pb atoms deposited on this substrate are not randomly distributed. The streakiness associated with figures 3(c) and (d) is related to the motion of adatom on the surface at $300\,\text{K}$. The grey arrows
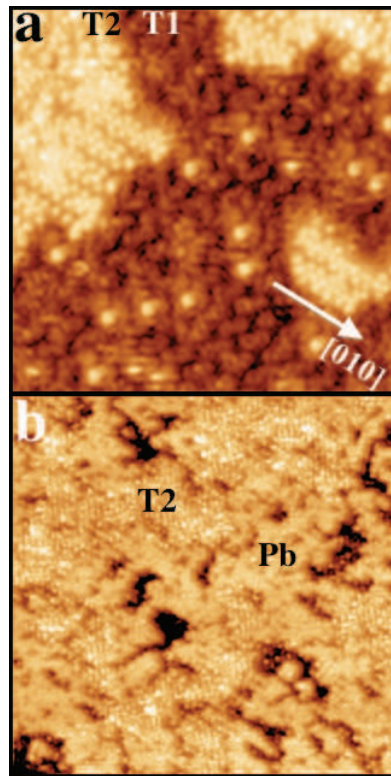
Figure 5. (a) High-resolution STM image $(20 \times 20\,\text{nm}^2)$ showing the surface structure after deposition of 0.38 MLE of Pb at 300 K on the $Al_{13}Co_4$ substrate. (b) STM image $(80 \times 80\,\text{nm}^2)$ recorded after 0.75 MLE Pb deposition. The T2 termination and the Pb region forming the first ML are indicated by T2 and Pb.

on both STM images point to a stable adsorbate over the scanning period. The white arrows demonstrate that an empty site is populated over a few minutes. At this stage, we cannot rule out that this effect is related to a tip-induced motion. To identify the precise nucleation site of Pb atoms on the bipentagonal motifs, a 2D grid has been superimposed on the T1 termination (figure 4(a)). The lines of the grid follow the diagonals of the $Al_{13}Co_4$ unit cell. The grid vertices are located exactly in between the two small pentagons forming the bipentagonal motifs (see the detailed arrangement in figure 4(b) where only 'protruding' bipentagonal motifs are drawn to replicate the STM observations). The brightest features corresponding to individual Pb atoms sit systematically on the grid nodes and hence above these bipentagonal motifs. The other set of vertices located above dark patches (the other type of bipentagonal motif) is not decorated by Pb atoms at this low coverage. A comparison of figures 4(a) and (b) suggests that Pb atoms are trapped in the hollow sites present between the two pentagons of the bipentagonal features (see the inset of figure 4(b)). Interestingly, the same site, as indicated by the arrows in figure 4(c), is sometimes decorated after a standard surface preparation by 'extra' atoms either intrinsic to the material or regarded as impurities (although undetectable by XPS). Thus, it is reasonable to consider these hollow sites as particularly reactive on the $Al_{13}Co_4(100)$ surface.

At 0.38 MLE coverage, the Z_{RMS} roughness, calculated for the combined T2 and Pb structures, is measured at $0.46 \pm 0.06\,\text{Å}$. In addition to isolated adsorbates (see figure 5(a)), arrangement of Pb adatoms along a specific direction on the substrate leads to the formation of
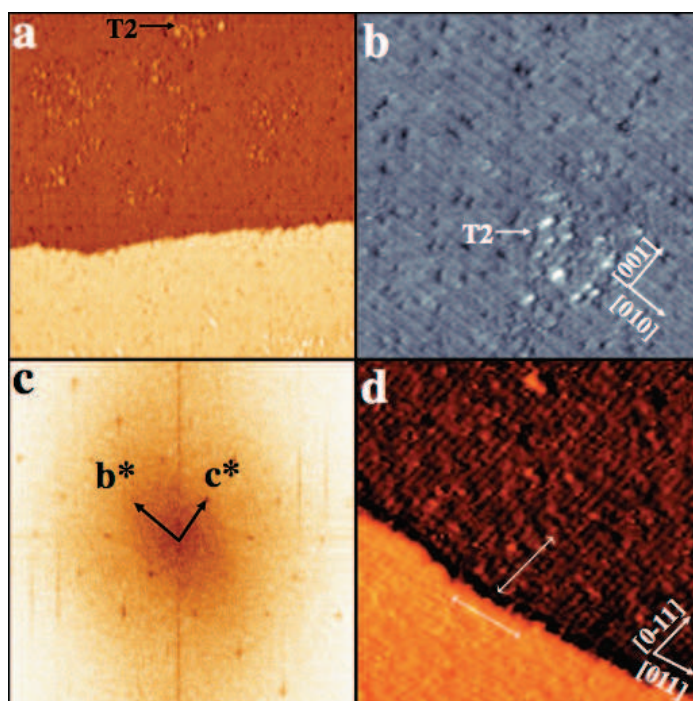
Figure 6. (a) STM image ($167 \times 167\,\text{nm}^2$) recorded after 1.5 MLE Pb exposure at 300 K on the $Al_{13}Co_4$ substrate. (b) STM image ($20 \times 20\,\text{nm}^2$) showing a complete layer composed of the Pb structure and T2 termination ($V_{bias} = -1.30\,\text{V}$, $I_t = 0.10\,\text{nA}$). (c) FFT calculated from the STM image presented in (b). (d) STM image ($40 \times 40\,\text{nm}^2$) recorded after 3 MLE Pb deposition at 300 K on the $Al_{13}Co_4$ substrate ($V_{bias} = -2.05\,\text{V}$, $I_t = 0.12\,\text{nA}$). As indicated by the double-head arrows, parallel lines are present on each terrace and are every second layer rotated by 80°.

a pronounced row structure. As presented on the high-resolution STM image in figure 5(a), this alignment corresponds to the [010] direction, i.e the closest in-plane distance between bipentagonal motifs (*b* axis). These 1D features have an apparent height that is very similar to that of the T2 termination, but can be well distinguished from the latter by their distinct structures. A majority of the Pb rows originate first from the edges of the fractioned T2 area. They can also spontaneously grow from the middle of the T1 layer as displayed in the bottom right-hand corner of figure 5(a). The average height difference between the substrate (T1) and the Pb structure is measured at 2.1 ± 0.1 Å. Upon further exposure (0.75 MLE), the first Pb ML is almost complete (figure 5(b)) with still no sign of the onset of the second layer growth. Regardless of their lateral width, all terraces are equivalently populated. Using higher-magnification STM images, a clear difference persists between the T2 and the Pb structures. Despite being well ordered as is evident from the previous LEED analysis, the contrast on the Pb region is lower than on the T2 patches at this coverage.

The STM image shown in figure 6(a) presents two terraces separated by a single step height after 1.5 MLE Pb exposure. The surface is now well covered by a thin (non-continuous) Pb ML. A closer inspection reveals that some structural defects (vacancy-like depressions for instance) remain within the deposited film. The pores observed at this coverage represent $4.0 \pm 0.4\%$
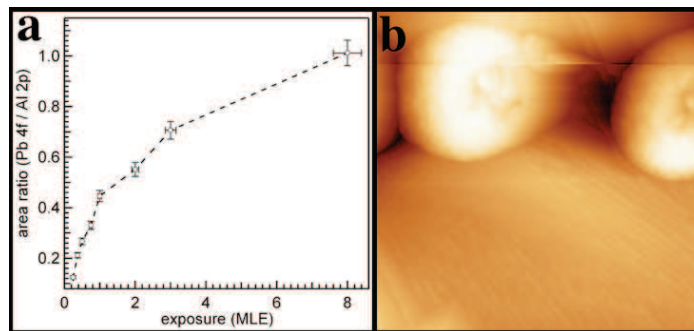
Figure 7. (a) The area under the peak ratio for Pb 4f to Al 2p as a function of the adsorbate exposure. The uncertainty in the deposition and area ratio is estimated around $\pm 5\%$. (b) STM image (167×167 nm^2) showing Pb mounds on the substrate after 3 MLE Pb exposure.

of the total scanned area. As shown by the arrow in figure 6(b), patches of T2 termination can still be easily identified. The FFT calculated from this image (see figure 6(c)) exhibits a large number of sharp spots and a rectangular unit cell in perfect agreement with the LEED measurements, which suggest a pseudomorphic Pb growth mode. Within the Pb region, the STM resolution in figure 6(b) allows us to distinguish parallel atomic lines spaced by ~ 15 Å along the [001] direction, i.e. comparable to the lattice parameter c. As expected, these latter do not rotate from one terrace to the next as they are related to the row structures aligned along the [010] direction observed at sub-ML coverage. At 3 MLE exposure, parallel lines separated by 10 ± 1 Å, which is equivalent to half of the diagonal of the surface unit mesh, are more easily distinguishable (see figure 6(d)). These atomic lines are rotated by $80°$ on successive terraces. Different tip conditions and/or a denser film (fewer depressions at 3 MLE exposure) could explain the emphasis of these rotating lines on the STM image at the expense of those visible in figure 6(b). On the clean surface, the lines interconnecting the bipentagonal motifs along the [011] or [0 − 11] directions have a spacing of ~ 10 Å, hence explaining the above measurements. In addition, they rotate by an identical amount on adjacent terraces separated by a single step height [18]. As these features can be related to the substrate underneath, this implies that a surface reconstruction, if any, must be minimum at the interface. The Z_{rms} for this coverage is about 0.22 ± 0.03 Å. The investigation of all the STM images recorded for this coverage reveals a total absence of individual adatoms or Pb islands forming the second ML.

3.2.3. X-ray photoelectron spectroscopy (XPS) analysis. To fully characterize the growth mode of Pb adatoms on the Al$_{13}$Co$_4$(100) surface, XPS measurements have been carried out for each exposure. The area ratio of the adlayer (Pb 4f) to the substrate signal (Al 2p) is plotted in figure 7(a) as a function of Pb exposure. While the substrate signal (Al 2p) is steadily decreasing, the adlayer signal (Pb 4f) increases continuously up to 1 MLE. Above this exposure, the rate of increase is reduced but remains almost linear up to the highest Pb depositions. Similar behaviour has been observed for the layer-by-layer growth of Pb on the Al(111) surface [15]. However in our study, STM images clearly show the absence of growth of a second ordered layer. Only one complete pseudomorphic Pb ML has been deposited up to the highest Pb exposure used in our study. Large (2–8 nm high and 50–60 nm wide) Pb mounds have been frequently observed in
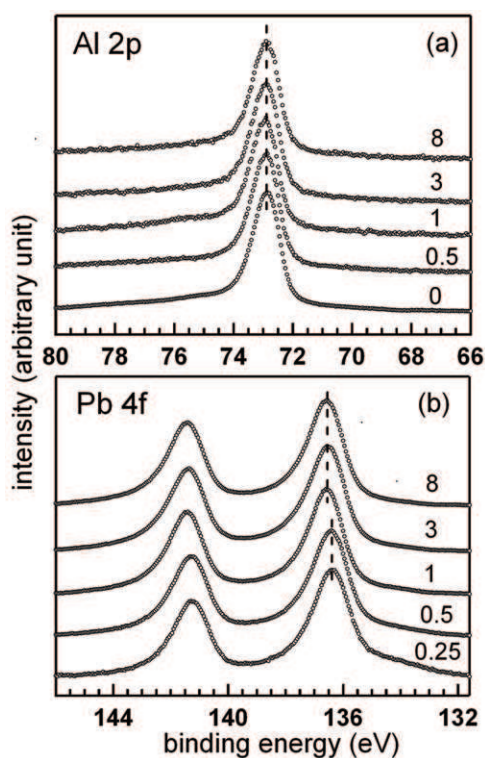
Figure 8. (a) The Al 2p core level spectra as a function of Pb exposure on the $Al_{13}Co_4(100)$ surface. (b) The Pb 4f core level spectra as a function of Pb exposure. In each case, the spectra have been normalized to have the same peak height and stacked along the vertical axis. The Pb exposures are indicated in terms of MLE on the right-hand side of the spectra.

the STM images (see figure 7(b)). These features are thought to correspond to agglomeration, probably at defect sites, of Pb adatoms diffusing across the terraces when the first layer has been completed. The growth of such Pb mounds will be favoured upon additional Pb exposure. Consequently, the Pb/Al area ratio signal should continuously increase as observed by XPS measurements (figure 7(a)). It clearly indicates that the growth of additional layers on the pseudomorphic Pb ML is prohibited above 1 MLE exposure. Upon further deposition, the lateral growth of these Pb mounds should eventually cover a larger part of the films. This would lead to an increase in the LEED background (see figure 2(d)).

Figure 8(a) shows the evolution of the Al 2p core level spectra as a function of Pb exposure. All the spectra have been normalized to have the same peak height, which enables us to track any changes in the core level lineshape and position with increasing exposure. The binding energy (BE) of Al 2p measured at 72.9 eV is not modified during the deposition. Similarly, the core level lineshape (broadening) of Al 2p is not altered upon Pb dosage. The Pb 4f core level spectra as a function of Pb exposure is presented in figure 8(b). Up to 1 MLE, the Pb 4f core level shifts towards higher BEs. Its BE equal to 136.35 ± 0.05 eV for the lowest coverage (0.25 MLE) reaches finally 136.55 ± 0.05 eV with the completion of the ML. For exposures $\geqslant 1$ MLE, the Pb 4f core level position is not shifted ($= 136.55$ eV, this value corresponds to the bulk Pb 4f) and the Pb 4f core level lineshape is not modified either.
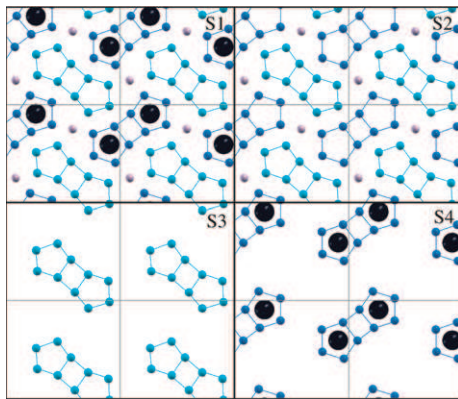
Figure 9. The $Al_{13}Co_4(100)$ surface models S_1 to S_4 shown in a 2×2 surface unit cell. The bipentagonal pattern slightly above the mean position of the topmost atomic layer ('protruding') is shown in dark blue (black), while the bipentagonal pattern slightly below the mean position of the topmost atomic layer is shown in cyan (grey). The Al atoms are the small spheres and the Co atoms are the large spheres.

3.2.4. Submonolayer (sub-ML) Pb adsorption studied by ab initio calculations. To analyse the initial growth mode of Pb adatoms on this surface, relative adsorption energies have been calculated for different sites i on the $Al_{13}Co_4$ surface using the following equation:

$$\Delta E^{(i)} = E^{(i)}_{\text{slab+Pb}} - E^{(4)}_{\text{slab+Pb}}, \tag{1}$$

where $E^{(i)}_{\text{slab+Pb}}$ is the total energy of the system (slab+adsorbed Pb at site i). Several possible surface models resulting from the preliminary study of the clean surface have been considered here [18, 25]. This should result in different initial adsorption sites across the incomplete $Al_{13}Co_4(100)$ topmost layer, each site presenting a different atomic environment. The four different surface models selected are described using figure 9. The model S_1 considers a dense Al-rich termination (22 Al and 2 Co atoms), while the S_2 surface (22 Al atoms) is obtained by removing all surface Co atoms. The S_3 (10 Al atoms) and S_4 (10 Al and 2 Co atoms) models correspond, respectively, to surfaces where only one set of bipentagonal motifs, either empty or containing Co atoms, has been preserved.

With this precision estimated in section 2.2 and due to computational limitations, a 6-layer-thick slab has been used to evaluate the adsorption energies for the different configurations (S_{1-4}). From the several calculations performed, only the relative adsorption energies obtained on the surface model S_2 are presented in table 1. Two types of attractive adsorption sites have been highlighted: (i) at the centre of each bipentagonal motif (labelled 2 and 4) and (ii) as fivefold and fourfold sites in between the bipentagonal patterns (labelled 5, 6, 7 and 8). The fivefold sites 1 and 3 (the centre of pentagons) and site 9 are all clearly unfavourable. The hollow site in between the two pentagons forming the 'protruding' bipentagonal motif (site 4) has been identified by the calculations as one of the favoured adsorption sites and it is indeed preferentially populated upon Pb adsorption. However, there exists a discrepancy for the decoration of sites 2, 7 and 5 which appear to remain vacant at the lowest Pb coverage from our STM measurements. Similarly, the 'dark stars' (surface vacancies) present on the fivefold Al–Pd–Mn quasicrystalline surface, which emerge among the potential adsorption sites
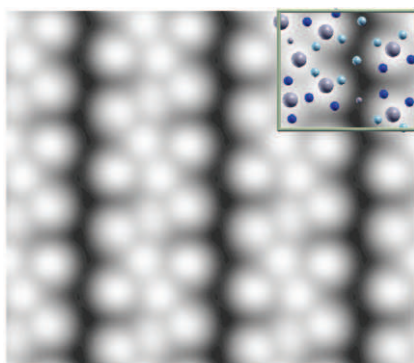
Figure 10. Simulated STM image $(-0.5\,V)$ exhibiting rows of Pb adatoms aligned along the [010] direction on the $Al_{13}Co_4(100)$ surface (S_2 model) at a coverage of 0.4 MLE. One unit cell has been highlighted where the largest spheres (grey) correspond to Pb adatoms. The Al atoms belonging to the 'protruding' bipentagonal pattern are shown in dark blue (black), while the Al atoms belonging to the other bipentagonal pattern are shown in light blue (grey). The two Al glue atoms are represented by the smallest spheres (light grey).

from the calculations, are not initially decorated by Pb adatoms at 57 and 300 K [14]. These differences between simulation and experimental observations could be related to a temperature effect and/or to the limitations of the present calculations. For the remaining configurations (S_1, S_3 and S_4), the calculations do not lead to the initial preferential adsorption site determined experimentally. For instance, the relative adsorption energy difference between site 4 (located in between two Co atoms) and site 2 (the centre of the Co-free bipentagonal motifs) is equal to 0.35 eV for the S_1 model. It is even larger when comparing sites 4 and 5 for the same configuration (0.45 eV).

For a coverage of 0.38 MLE, lines of Pb atoms oriented in the [010] direction appear on the experimental STM image (see figure 5(a)). To interpret this experimental result, models have been built by decorating the preferential adsorption sites (4, 6, 7, 8 and geometrically equivalents) identified by the calculations for the S_1 and S_2 models. Due to their lower plane density, different adsorption sites have been considered for the S_3 and S_4 models. They correspond to positions 2, 1, 5, 8 (resp. 4, 8, 7, 1) and geometrically equivalents for the S_3 (resp. S_4) configuration. The resulting STM images for the S_1 and S_2 models are in good agreement with the experimental images (see figure 10). However, these row structures have not been reproduced using the S_3 and S_4 models and the corresponding initial Pb positions described previously.

To summarize, these calculations have highlighted that the initial nucleation site and the Pb row structures could both be reproduced using the S_2 model. The adsorption site obtained experimentally does not emerge as a favoured site for the three other surface models. This computational approach allows us to discriminate among several surface models initially thought to be potential candidates. Thus, this Pb adsorption study tends to confirm the validity of the S_2 model described by Shin *et al* [25] and presented in table 1 to describe the $Al_{13}Co_4(100)$ surface structure.
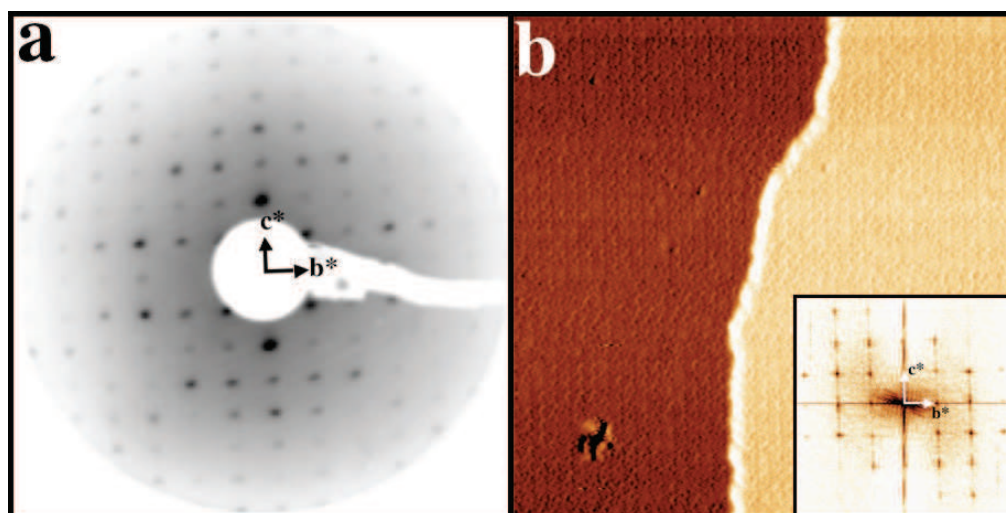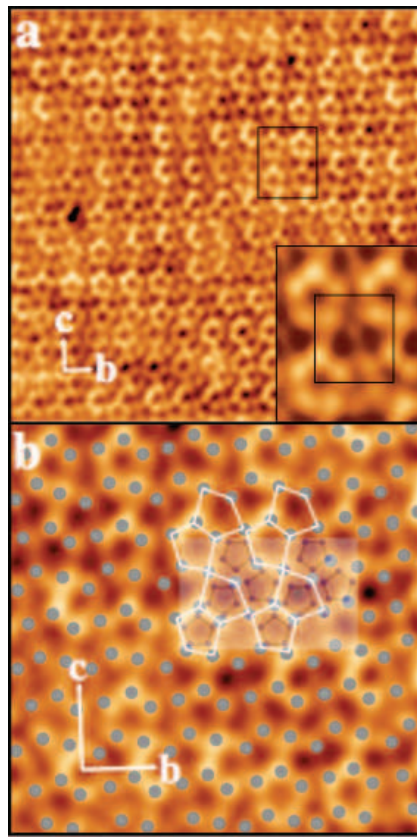
Figure 11. 1 MLE Pb has been deposited at 573 K on the $Al_{13}Co_4$ substrate. (a) LEED pattern (inverted for clarity) recorded at 65 eV beam energy. (b) STM image (50×50 nm^2) showing two terraces which exhibit fine structural details (inset: FFT calculated from the STM image in (b)). An atomically resolved STM image obtained on one of these terraces is presented in figure 12.

3.3. Pb deposition at 573 K

To improve the structural ordering within the Pb thin film, the $Al_{13}Co_4$ sample has been kept at 573 K during the 1 MLE deposition. The corresponding LEED pattern (see figure 11(a)) is consistent with a pseudomorphic growth mode of Pb adatoms. The lattice parameter ratio ($(\frac{c}{b})_{measured} = 1.154$) extracted from this LEED pattern is close, within the accuracy of our measurements, to that reported by Grin *et al* ($(\frac{c}{b})_{bulk} = 1.171$) [26]. Compared to room temperature deposition (see figure 2(b)), there is a remarkable enhancement in the quality of the diffraction pattern. As shown in figure 11(b), terraces are now completely covered by a Pb thin film, with no sign of a second layer growth. In this region of the sample, the widths of the terraces prohibit the presence of the T2 terminations [18]. The structural quality of the film is indeed improved as revealed by the reduced percentage of pores within the ML and the relatively low roughness, with Z_{rms} measured at 0.16 ± 0.04 Å. Figure 11(b) exhibits fine structural details distributed periodically on both terraces. To determine the lattice parameters of this ML, an FFT has been calculated from figure 11(b). The size of the orthorhombic unit cell has been measured with $b = 12.59 \pm 0.50$ Å and $c = 14.76 \pm 0.70$ Å, in agreement with the bulk parameters where $b = 12.342$ Å and $c = 14.452$ Å [26]. The LEED and FFT analyses demonstrate that the Pb thin film has adopted the underneath template lattice. Higher-resolution STM images are now required to investigate the local atomic arrangements of the adsorbates.

Figure 12(a) corresponds to an atomically resolved STM image recorded from one region of figure 11(b). The surface plane is mainly composed of pentagonal atomic arrangements distributed on a periodic network. Two sets of pentagons either pointing up or down with respect to the [001] direction can be defined. However, a majority of the most striking and discernable pentagons are those pointing upward. When the contrast is higher on the other set of pentagons (down), this leads to the impression of shifted atomic rows within the film. The variation and the

Figure 12. A complete Pb ML has been deposited at 573 K on the $Al_{13}Co_4$ substrate. (a) The high-resolution STM image ($18 \times 18 \, nm^2$) indicates that the structure is composed of pentagonal features. Inset: close-up view ($2.6 \times 3.2 \, nm^2$) of the rectangle displayed in (a). (b) Tiling using irregular pentagons of a region ($7.25 \times 7.25 \, nm^2$) extracted from the STM image presented in (a). The surface structure can be described as interconnected bipentagonal motifs (see white pentagons). To analyse the ML formed, the structure of the P plan (bipentagonal motifs pointing in two directions and glue atoms) has been superimposed on the Pb structure.

inhomogeneous contrast present among the motifs (oriented up or down irrespectively) may be attributed to protruding adatoms which would result in a higher intensity locally in the image. Such local height variations of the adsorbates may result either from local defects (within the film or on the substrate) or from a buildup of strain, partly relieved by a small buckling of the ML.

The unit cell dimensions of this structure ($b = 12.72 \pm 0.50 \, Å$ and $c = 14.58 \pm 0.70 \, Å$) match those of the clean substrate. As seen from one unit cell outlined in the inset of figure 12(a), the pentagons are not regular in shape regardless of their orientation. In fact, their edge lengths vary between 4.1 and 6.1 Å, with a mean value estimated at 4.83 Å. Interestingly, the ratio of this average value to the mean edge lengths (2.88 Å) of the pentagons forming the bipentagonal motif on the clean surface is equal to ~1.67, i.e. very close to the golden mean $\tau (= 1.618\ldots)$. The film structure has been analyzed using a tiling approach. Each bright contrast within

one unit cell has been associated with a Pb adatom. The resulting arrangement, distributed periodically across the surface plane (figure 12(b)), leads to an interpretation of the thin film structure as being composed of connected bipentagonal motifs. This arrangement is obviously closely related to the clean surface, which consists of smaller bipentagonal motifs (see, for instance, figure 4(c)). When attributing a Pb atom to each vertex of the tiling, the apparent density of the film is lower (0.034 atom Å^{-2}) than the value measured using XPS. The latter is comparable to the densities reported while dosing 1 ML of Pb on the Al(111) and the fivefold i-Al–Pd–Mn surface, i.e. 0.09 atom Å^{-2} [15]. As a first attempt to understand the structural relationship that exists between the ML and the substrate, the structure of the puckered P layer has been superimposed on the Pb layer. Due to the different possible alignments between the two structures, the bipentagonal motifs have been arbitrarily placed inside the large bipentagons formed by the Pb atoms. In this particular configuration, the 'glue' atoms of the puckered P plan coincide with the Pb atoms shared between the large bipentagon (white pentagons in figure 12(b)). Further experimental studies (dynamical LEED I–V for instance) coupled with simulated STM images (generated from *ab initio* calculations) are necessary to validate the proposed superposition and to refine the film structural model. Thus, the bipentagonal motifs present on the bare surface must also play a crucial role in the formation of the Pb ML at 573 K. The LEED and STM analyses demonstrate that the growth of Pb adatoms on the Al$_{13}$Co$_4$ substrate is pseudomorphic from 300 to 573 K.

4. Discussion

We have characterized the adsorption of Pb atoms on the Al$_{13}$Co$_4$(100) surface. Pb adatoms adsorb initially in hollow sites located in the centre of bipentagonal motifs, i.e. in between neighbouring caps of the pentagonal bipyramid clusters [18, 26]. In time series STM images, diffusion of the Pb atoms can be observed, indicating their high mobility on the surface at sub-ML coverage. Upon further deposition, we observe the formation of small Pb islands that grow with a row structure preferentially along the [010] direction. The step edges of the remaining T2 termination act also as defect sites for Pb nucleation. Upon the completion of the first ML, it is not possible within the deposition flux used (4.2 × 10^{-3} ML s^{-1}) in our study to grow a second layer. Both LEED and STM analyses indicate a pseudomorphic growth mode. This adsorption behaviour is to be compared with previous adsorption works carried out on aperiodic surfaces [10, 13, 15]. A preferential nucleation site has also been identified for Pb adsorption on the i-Al–Pd–Mn fivefold surface. It corresponds to equatorially dissected clusters known as pseudo-Mackay clusters. The decoration of these unique adsorption sites leads to the formation of pentagonal islands (Pb$_{10}$) dubbed 'starfish' and eventually to a quasiperiodic Pb ML.

On periodic or aperiodic CMA surfaces, the clusters appear to play a crucial role at the initial stages of the nucleation. Their density and inter-distances on terraces may be the decisive parameters to obtain a pseudomorphic ML. The Pb mobility seems comparable on approximant and aperiodic surfaces. In addition, the surface relaxation of the quasicrystalline substrate is thought to be minimum upon Pb adsorption [27]. On the Pb ML adsorbed on the Al$_{13}$Co$_4$ surface, the fine structures that rotate by 80° from successive terraces are directly related to the orientation of the underneath bipentagonal motifs. Hence, it is likely that the same conclusion can be drawn regarding the surface relaxation of the approximant, but additional measurements would be required to ascertain this point.

For the $Al_{13}Co_4$ surface, it was not possible to grow a second ordered layer once the completion of the first pseudomorphic ML has been achieved. As mentioned above, this trend is consistent with what has been reported on terraces of quasicrystalline surfaces [10, 15]. The energy position and lineshape (absence of any extra component or broadening) of the Al 2p core level remain unchanged with increasing exposure, which suggests a weak interaction between the Pb and Al atoms. This phenomenon is expected considering the bulk immiscibility of Pb and Al [28, 29]. Similar behaviour of the Al 2p peak has been observed in previous works about Pb adsorption on quasicrystalline and on Al(111) surfaces [10, 13, 15]. The small shift $(0.20 \pm 0.05 \, eV)$, measured on the Pb 4f core level below 1 MLE, may be due to substrate-related initial or final state effects. At sub-ML coverages, the Pb 4f core-hole may be strongly screened by the Al conduction electrons, which could eventually reduce the BE of the Pb 4f core level.

For higher-temperature deposition, the quality of the LEED patterns is clearly improved, which suggests greater structural ordering within the Pb thin film. This is indeed the case as demonstrated by the atomically resolved STM images. The structure of the film is described by a periodic arrangement of irregular pentagons of average edge lengths equal to 4.8 Å. This dimension is similar to several pentagonal features present within the pseudomorphic Pb films formed on the i-Al–Pd–Mn and d-Al–Ni–Co [13, 27]. The Pb structure can tentatively be understood as connected bipentagonal motifs, which are larger than those observed on the clean $Al_{13}Co_4$ surface. Compared to the 'isolated' Al bipentagonal motifs present on the clean surface, the Pb bipentagons share several common vertices. This is a direct consequence of the larger adsorbate atomic size compared to Al atoms.

Consequently, these results demonstrate that Pb adsorption on the $Al_{13}Co_4(100)$ surface reproduces the main trends observed on quasiperiodic surfaces (pseudomorphy, heterogenous nucleation, mobility and growth of additional layer inhibited). For the Al(111)/Pb system [15], the inter-adsorbate interaction dominates the growth mode and leads to the formation of a moiré pattern. In the case of $Al_{13}Co_4(100)$ with only Al atoms within the topmost layer, the adsorbate–substrate interaction (via the surface clusters) plays a dominant role in the initial growth of Pb adatoms. Then, the adsorbate–adsorbate interaction is required to stabilize the motifs observed in the sub-ML regime. While being a periodic surface, this adsorption study on $Al_{13}Co_4(100)$ shows that the pertinent length scale remains the (inter-)clusters dimensions for the growth mode of Pb adatoms.

5. Conclusions

We have investigated the deposition of Pb adatoms on the p–10f $Al_{13}Co_4(100)$ surface. Pb adsorption follows a pseudomorphic growth mode up to one ML. There is no sign of intermixing or alloy formation upon Pb dosing. A preferential nucleation site has been identified for the initial stage of adsorption, hence resulting in inhomogeneous nucleation. It corresponds to the hollow site or centre of the bipentagonal motifs present across terraces. The experimental results are supported by *ab initio* calculations. With further dosage, Pb islands show a row structure and extend initially along the [010] direction. Above one ML, the high diffusion length of Pb across atomically flat terraces of the $Al_{13}Co_4$ surface limits the growth of additional layers. Deposition of the adsorbates with the sample held at 573 K leads to enhanced structural ordering within the Pb adlayers. The ML can then be described using a tiling based on bipentagonal motifs.

IOP Institute of Physics **Φ** DEUTSCHE PHYSIKALISCHE GESELLSCHAFT

Acknowledgments

References

[1] Tsai A P, Guo J Q, Abe E, Takakura H and Sato T J 2000 *Nature* **408** 537
[2] Takakura H, Gómez C P , Yamamoto A, De Boissieu M and Tsai A P 2007 *Nat. Mater.* **6** 58
[3] Franke K J, Sharma H R, Theis W, Gille P, Ebert P and Rieder K H 2002 *Phys. Rev. Lett.* **89** 156104
[4] Ledieu J, Hoeft J-T, Reid D E, Smerdon J A, Diehl R D, Lograsso T A, Ross A R and McGrath R 2004 *Phys. Rev. Lett.* **92** 135507
[5] Sharma H R, Shimoda M, Ross A R, Lograsso T A and Tsai A P 2005 *Phys. Rev. B* **72** 45428
[6] Krajčí M and Hafner J 2005 *Phys. Rev. B* **71** 184207
[7] Curtarolo S, Setyawan W, Ferralis N, Diehl R D and Cole M W 2005 *Phys. Rev. Lett.* **95** 136104
[8] Krajčí M and Hafner J 2007 *Phys. Rev. B* **75** 224205
[9] Krajčí M and Hafner J 2008 *Phys. Rev. B* **77** 134202
[10] Ledieu J, Leung L, Wearing L H, McGrath R, Lograsso T A, Wu D and Fournée V 2008 *Phys. Rev. B* **77** 073409
[11] Smerdon J A, Parle J K, Wearing L H, Lograsso T A, Ross A R and McGrath R 2008 *Phys. Rev. B* **78** 075407
[12] Setyawan W, Diehl R D and Curtarolo S 2009 *Phys. Rev. Lett.* **102** 055501
[13] Smerdon J A, Leung L, Parle J K, Jenks C J, McGrath R, Fournée V and Ledieu J 2008 *Surf. Sci.* **602** 2496
[14] Ledieu J, Krajčí M, Hafner J, Leung L, Wearing L H, McGrath R, Lograsso T A, Wu D and Fournée V 2009 *Phys. Rev. B* **79** 165430
[15] Deniozou Th, Ledieu J, Fournée V, Wu D M, Lograsso T A, Li H I and Diehl R D 2009 *Phys. Rev. B* **79** 245405
[16] Buchanan J D R, Hase T P A, Tanner B K, Chen P J, Gan L, Powell C J and Egelhoff W F 2002 *Phys. Rev. B* **66** 104427
[17] Otero R, Vazquez de Parga A L and Miranda R 2002 *Phys. Rev. B* **66** 115401
[18] Addou R *et al* 2009 *Phys. Rev. B* **80** 014203
[19] Kresse G and Furthmüller J 1996 *Phys. Rev. B* **54** 11169
[20] Kresse G and Furthmüller J 1996 *Comput. Mater. Sci.* **6** 15
[21] Blöchl P E 1994 *Phys. Rev. B* **50** 17953
[22] Kresse G and Joubert D 1999 *Phys. Rev. B* **59** 1758
[23] Perdew J P, Burke K and Ernzerhof M 1996 *Phys. Rev. Lett.* **77** 3865
[24] Perdew J P, Burke K and Ernzerhof M 1997 *Phys. Rev. Lett.* **78** 1396
[25] Shin H *et al* 2011 *Phys. Rev. B* **84** 085411
[26] Grin J, Burkhardt U, Ellner M and Peters K 1994 *J. Alloys Compd.* **206** 243
[27] Krajčí M and Hafner J 2009 *Phys. Rev. B* **80** 214419
[28] Johnson E, Johansen A, Dahmen U, Chen S and Fujii T 2001 *Mater. Sci. Eng.* A **304–306** 187
[29] Matolín V, Matolínová I, Tsud N, Fabík S, Libra J, Dudr V, Cháb V and Prince K C 2006 *Phys. Rev. B* **74** 075416